JACS
JOURNAL OF THE AMERICAN CHEMICAL SOCIETY

Article

pubs.acs.org/JACS

Bioactive Surface Modification of Metal Oxides via Catechol-Bearing Modular Peptides: Multivalent-Binding, Surface Retention, and Peptide Bioactivity

Wen Tang,[†] Gina M. Policastro,[†] Geng Hua,[†] Kai Guo,[†,‡] Jinjun Zhou,[†] Chrys Wesdemiotis,[†,‡] Gary L. Doll,[§] and Matthew L. Becker*[,†]

[†]Department of Polymer Science, The University of Akron, Akron, Ohio 44325, United States

[‡]Department of Chemistry, The University of Akron, Akron, Ohio 44325, United States

[§]Timken Engineered Surfaces Laboratory, Department of Civil Engineering, The University of Akron, Akron, Ohio 44325, United States

Supporting Information

ABSTRACT: A series of multivalent dendrons containing a bioactive osteogenic growth peptide (OGP) domain and surface-binding catechol domains were obtained through solid phase synthesis, and their binding affinity to hydroxyapatite, TiO_2, ZrO_2, CeO_2, Fe_3O_4 and gold was characterized using a quartz crystal microbalance with dissipation (QCM-d). Using the distinct difference in binding affinity of the bioconjugate to the metal oxides, TiO_2-coated glass slides were selectively patterned with bioactive peptides. Cell culture studies demonstrated the bioavailability of the OGP and that OGP remained on the surface for at least 2 weeks under in vitro cell culture conditions. Bone sialoprotein (BSP) and osteocalcein (OCN) markers were upregulated 3-fold and 60-fold, respectively, relative to controls at 21 days. Similarly, 3-fold more calcium was deposited using the OGP tethered dendron compared to TiO_2. These catechol-bearing dendrons provide a fast and efficient method to functionalize a wide range of inorganic materials with bioactive peptides and have the potential to be used in coating orthopaedic implants and fixation devices.

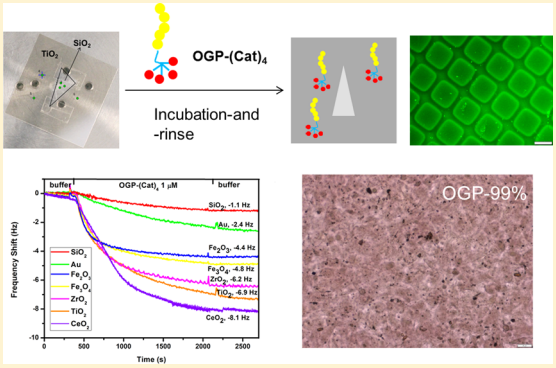

INTRODUCTION

Immobilization of bioactive peptides onto surfaces has been proven to be an effective avenue to improve cell attachment,[1] influence proliferation,[2] and direct differentiation in tissue engineering.[3,4] Physical adsorption/encapsulation and chemical conjugation have both been applied to derivatize tissue engineering scaffolds with bioactive peptides.[5−9] Most of these methods were developed for polymeric materials, while the surface decoration of inorganic surfaces has received less attention, due to the lack of diversity in presenting functional groups for highly efficient chemical reactions.[10−12] However, many inorganic materials are useful in the medical applications field. For instance, titanium and zirconia are widely used in prosthetic devices and dental implants;[13,14] cerium oxide nanoparticles are potent antioxidants in therapeutics;[15,16] and iron oxide magnetic nanoparticles are used to enhance the magnetic resonance imaging contrast in disease diagnostics.[17] Thus, the development of efficient and convenient methods to immobilize bioactive peptides onto the surface of metal oxide materials (TiO_2, ZrO_2, CeO_2, Fe_3O_4 and so on) will not only influence the cell behavior locally but will also contribute to the improvement of diagnostic and therapeutic techniques in the clinic.[18]

Titanium is the most widely used material in bone implants and dental fixations due to its low density, high strength and high resistance to erosion. In physiological conditions, the oxide passivation layer of 2−20 nm TiO_2 is quickly formed on titanium implants.[19] Several methods have been developed to decorate titanium implants with bioactive peptides/proteins. Modifications can be achieved through physical interactions, such as protein-encapsulated coating,[20] erosion and subject protein adsorption,[21] and peptide-grafted polycation adsorption.[22] However, the diffusion of loaded bioactive components may require high doses, and lead to low drug efficiency, and other adverse reactions.[23−26] Chemical conjugation by generating reactive functional groups using electrochemical anodization,[27] acid-etching,[28] and oxidation,[29,30] have been utilized to covalently conjugate the bioactive moieties onto the titanium implant surface, which requires complicated procedures and changes the surface properties during the fabrication.

The presence of 3,4-dihydroxyphenylalanine (DOPA), which is found abundantly in mussel adhesive proteins, has been connected to the strong adhesion of mussels onto multiple

Received: August 29, 2014
Published: October 24, 2014

dx.doi.org/10.1021/ja508946h | J. Am. Chem. Soc. 2014, 136, 16357−16367

Scheme 1. Molecular Structures of OGP-(Cat)$_n$ and OGP-PEG-(Cat)$_n$, n = 1, 2, 4

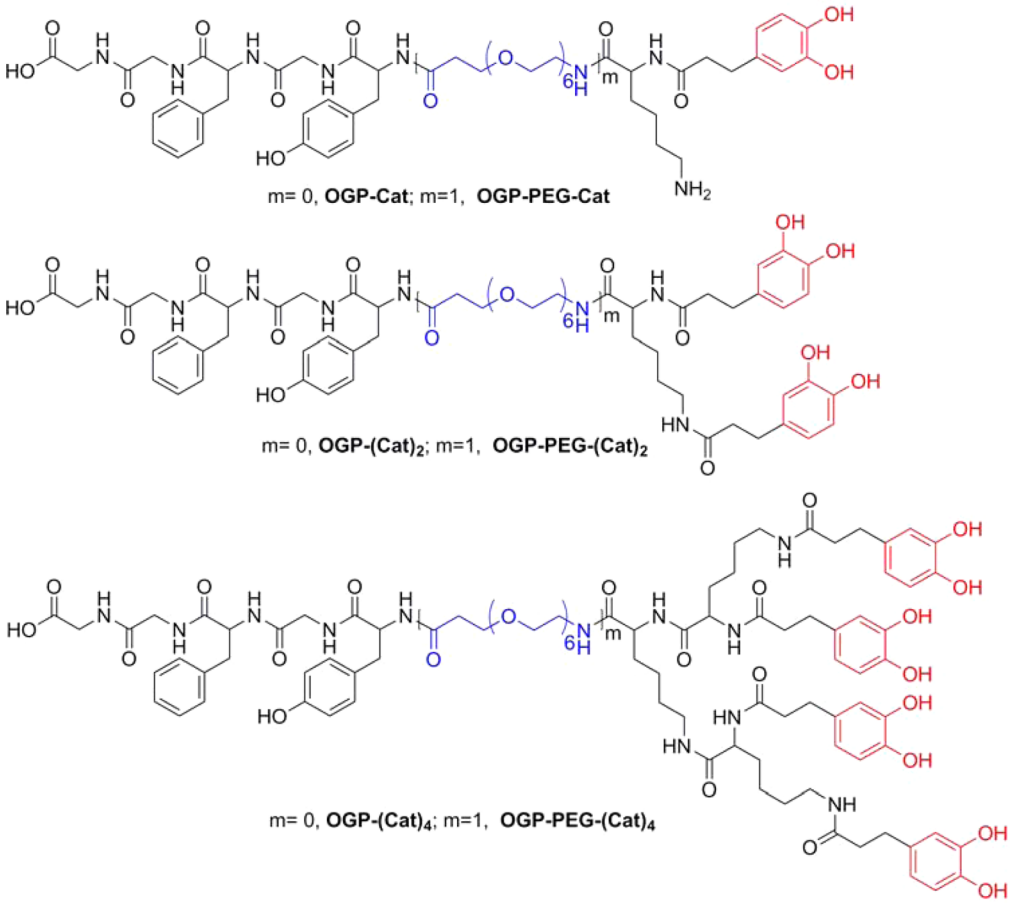

surfaces in wet conditions.[31] Catechol group is the functional group of DOPA, which is known to interact with titanium oxide surface through coordination bond or H-bond with pH sensitivity.[32−34] Catechol is also cross-linked together under oxidative or basic conditions to form coating layers on surfaces.[33] Thus, it has served as adhesive building blocks in the surface coating of a variety of materials, including metal oxides, as well as organic polymers.[35−38] Besides titanium oxide, the interaction of catechol with other metal oxides has also been studied, including iron oxide,[39] chromium(III) oxide,[40] manganese dioxide,[40] aluminium oxide[41] and zirconia.[41] Antifouling ethylene glycol dendrons[42] and glycocalyx[43] layers have been successfully coated onto titanium oxide surfaces with catechol-functionalized oligomers as the surface-anchoring domain in the pioneered work. However, sequestering bioactive moieties, such as peptides that are known to direct cell behaviors, with catechol-bearing molecules on the surfaces of biomaterials has not been reported.

Modular peptides are conjugated molecules containing several different peptide sequences that are known to have specific biofunctionality. The Murphy group has successfully applied this molecular design in the modification of hydroxyapatite surfaces with osteoconductive peptides using a cost-effective dip-and-rinse procedure.[44−46] In the modular peptides, there are two active components, the surface-binding peptide that sequesters the whole molecule on the hydroxyapatite surface and the bioactive subunit that influences the cell behavior. The loading concentration and retention time of the peptides on the surface are critical parameters that determine whether molecular signaling in the cell will be triggered. In many studies it was shown that the cell response to specific peptides is concentration-dependent.[2,47] However, in most applications, the concentrations that are required to trigger and sustain the cell response are less understood. Strong adsorption is the prerequisite to realize efficient immobilization with bioconjugate solutions at low concentration, and to retain the peptides on the surfaces over extended periods. Thus, the key issue in the modification of surfaces with modular peptides is identifying the motifs that have strong binding affinity to the targeted surface and quantifying the binding affinity. Strategies and functional moieties that provide strong binding affinity are highly sought after.

Between two objects (e.g., molecules, proteins, surfaces of substrates and nanoparticles, cell membranes and so on), when there are more than one pair of ligand−receptor interaction binding simultaneously, a synergistic augment rises in binding affinity with an order of magnitude enhancement over the corresponding monovalent ligand.[48,49] This multivalent binding strategy has been used extensively in nature and synthetic molecules to enhance their respective binding affinity.[50−54] Dendrimers are ideal platforms to construct multivalent binding ligands due to their abundant functional groups in the periphery region.[55] Studies have shown that the molecular structure of the multivalent ligands, including binding valency,[56−58] the flexible linkage units,[59] molecular architecture[60,61] and receptor density[62] all play significant roles in the ultimate association constant of the multivalent ligand with its receptor. Models combining the macroscopic thermodynamics

dx.doi.org/10.1021/ja508946h | J. Am. Chem. Soc. 2014, 136, 16357−16367

Scheme 2. Fmoc Solid Phase Synthesis of OGP-PEG-$(Cat)_2$

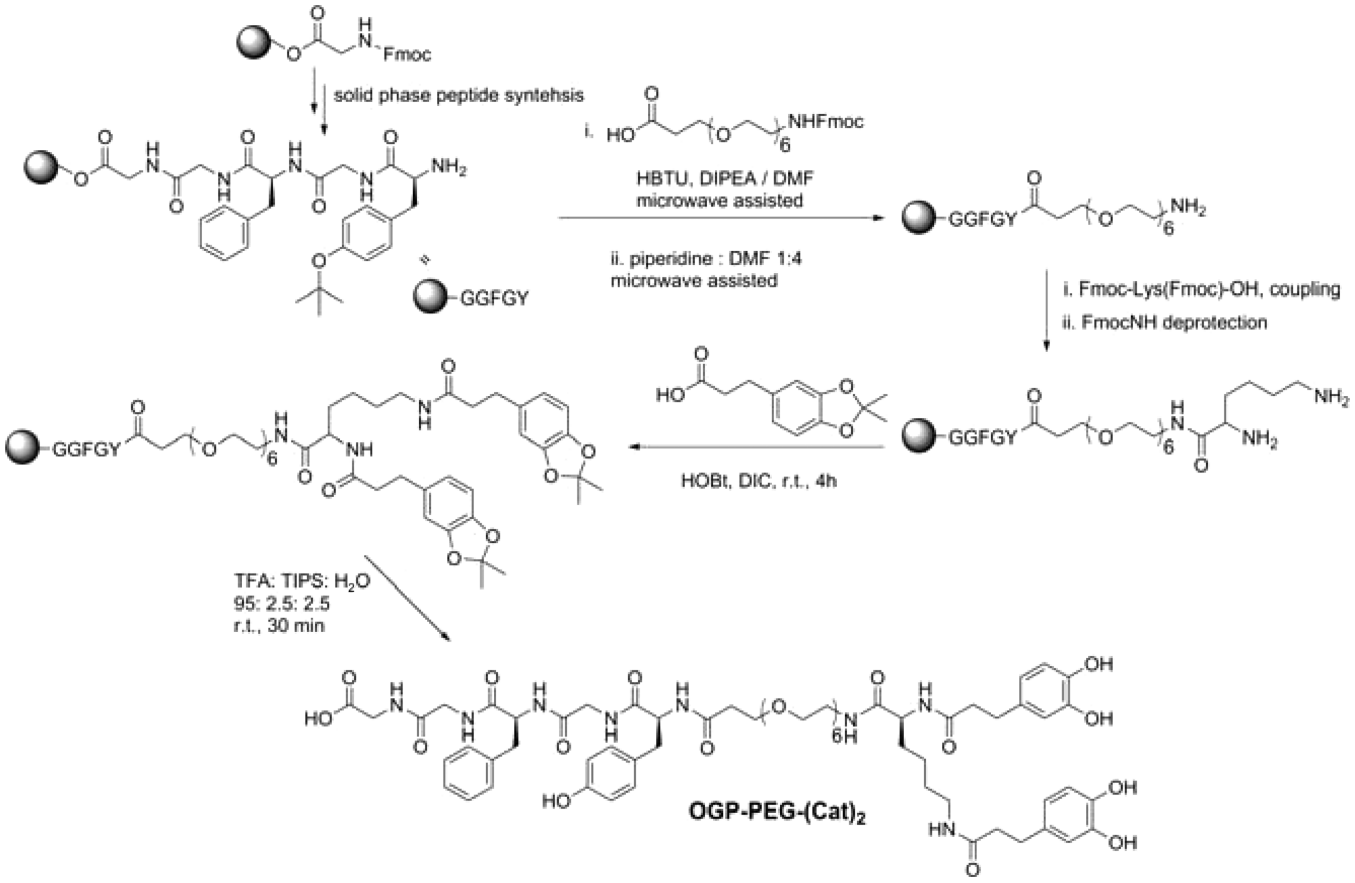

with microscopic probabilistic arguments based on the intramolecular reaction were employed to rationalize some experimental results.[63,64] The optimization of molecular structures for the strongest binding is important in the understanding of multivalent binding process, as well as the design of strong adhesive motifs for drug targeting and sequestering purposes.

Osteogenic growth peptide (OGP) is an endogenous regulatory tetradecapeptide present in mammalian serum with concentrations at the micromolar scale.[65] Native or synthetic OGP regulates proliferation, alkaline phosphatase activity and matrix mineralization in studies of osteoblastic cell lines derived from human and other mammalian species.[66] As its active portion, the carboxy-terminal pentapeptide, OGP(10−14) directs rat bone marrow mesenchymal stem cells to differentiate to osteoblasts.[66] OGP or OGP(10−14)-functionalized biomaterials, including scaffolds for bone tissue engineering,[67,68] gradient substrates,[2] and peptide nanofibers,[69,70] have been prepared, and shown to promote both cell proliferation and osteogenic differentiation, in vitro and in vivo. Therefore, OGP(10−14) is a good candidate to be utilized in our attempts to enhance the osteoinductivity of conjugate-derivatized metal oxide implants.

In this paper, a series of modular peptides containing bioactive OGP(10−14), and a multivalent catechol-functionalized dendron were synthesized using solid phase synthesis. The relationship between molecular structure, including binding valency (number of catechol groups in the molecule) and flexible linkage, and binding affinity was well elucidated to optimize the molecular structure for strong binding. The successful immobilization and retention time of peptides on the surface after a simple incubation-and-rinse procedure was studied using fluorescein-labeled peptides and X-ray photoelectron spectroscopy (XPS) analysis. The tetravalent ligand remained bioavailable on the surface in buffer at physiological pH for more than 2 weeks. The modular peptide exhibits strong interactions with several medically relevant materials (zirconia, cerium oxide, and iron oxide), demonstrating its usefulness in the surface modification of other biomedical devices. With the catechol-bearing modular peptides, selective surface modification was achieved on a patterned TiO_2-coated glass slide, which demonstrates a new method to fabricate surface with locally restricted peptides. The immobilized OGP(10−14) was able to stimulate cell proliferation and promote osteogenic differentiation and mineralization for MC3T3-E1 cells cultured on the substrates.

■ RESULTS AND DISCUSSION

Synthesis and Characterization of Catechol-Bearing Modular Peptides. Lysine-based dendrons were used as the platform to construct the catechol-bearing multivalent binding ligands with a bioactive peptide at the core as shown in Scheme 1. In the periphery of the dendron, tunable numbers of catechol (Cat) functional groups were attached with valencies equal to 1, 2, or 4. In the focal point of the dendron, an osteoconductive peptide, OGP(10−14), with the amino acid sequence YGFGG was linked. The two domains are connected with or without a hexaethylene glycol flexible linkage. We envision that the surface-binding domain will sequester the bioconjugate on the surface of metal oxide implants due to strong binding affinity,

dx.doi.org/10.1021/ja508946h | J. Am. Chem. Soc. 2014, 136, 16357−16367

and the bioactive domain will interact with cells and influence their behavior in a concentration dependent manner.

The synthesis of **OGP-(Cat)**$_n$ and **OGP-PEG-(Cat)**$_n$ (n = 1, 2, 4) were carried out using Fmoc based solid phase synthesis, and the synthesis of **OGP-PEG-(Cat)**$_2$ is shown in Scheme 2 as an example. The last coupling step of acetonide-protected 3,4-dihydroxyhydrocinnamic acids with amines in the peptide chain terminus cannot tolerate microwave-assisted conditions, and the protection of catechol groups is essential for successful synthesis. No intervening purification was required, and synthetic process only took 6 h in all. After RP-HPLC purification, the OGP(10−14) peptide-functionalized catechol-bearing dendrons were achieved with high purity with the yield of 9−25% as shown in ESI or MALDI-ToF mass spectrometry (Figure S1, Supporting Information).

Adsorption to TiO_2 Measured by QCM-d. The adsorption processes of all molecules to TiO_2 surfaces at 25 °C and pH 7.4 were monitored by quartz crystal microbalance with dissipation (QCM-d). Multivalent binding effects that enhanced the binding affinity were clear. In Figure 1, to obtain a similar level of adsorption, ~6 Hz frequency shift, the concentration of monovalent ligand, **OGP-Cat**, is 13 μM, while that of tetravalent ligand, **OGP-(Cat)**$_4$ and **OGP-PEG-(Cat)**$_4$, is 0.32 and 0.16 μM, respectively, due to the mass differences. A much smaller amount of sample (~80-fold less) is needed for the tetravalent ligand **OGP-PEG-(Cat)**$_4$ compared with the monovalent ligand **OGP-Cat** to achieve the same level (mass) of surface adsorption. Moreover, the tetravalent ligands remained on the TiO_2 surface under buffer washing, as no frequency shift was observed after switching the solution to HEPES buffer. This indicates that the tetravalent ligands are sequestered on the TiO_2 surface and are unlikely to diffuse away after being implanted into the body. Under similar conditions, the monovalent ligand was partially washed away. The adsorption kinetics were recorded by QCM-d, with regard to **OGP-PEG-(Cat)**$_4$, 2 h are needed to reach the equilibrium state at a concentration of 0.16 μM.

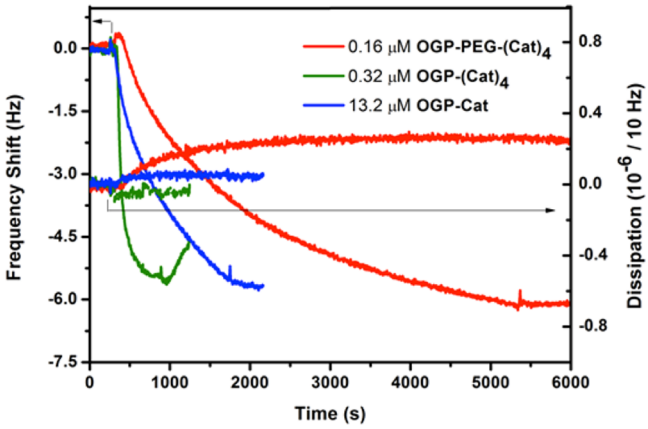

Figure 1. Adsorption of catechol-functionalized dendrons, **OGP-Cat**, **OGP-(Cat)**$_4$ and **OGP-PEG-(Cat)**$_4$ onto TiO_2 surface monitored by QCM-d. The experiment contains three processes: (i) baseline in HEPES buffer; (ii) adsorption of ligands; (iii) buffer washing the adsorbed ligands, as indicated by the small peak due to the stop of flow. To reach similar level of frequency shift, tetravalent ligands **OGP-(Cat)**$_4$ and **OGP-PEG-(Cat)**$_4$ requires solution at much lower concentration compared to monovalent ligand, **OGP-Cat**, indicating a stronger binding affinity. Signals from different overtones were close due to the rigidity of the adsorbed film, and those of n = 7 were shown here.

Binding Affinity and Maximum Adsorption. To quantitatively compare the binding affinities of the multivalent binding ligands, the adsorption properties at several different concentrations were measured. The solutions at higher concentrations were switched to flow above the sensor, until the adsorption of previous solution at lower concentration reached the equilibrium state (the change in frequency shift is smaller than the signal fluctuation, 0.05 Hz/min), taking **OGP-Cat** as an example shown in Figure 2A. The corresponding frequency shift was calculated using Sauerbrey equation to get the adsorbed area mass. The adsorption isotherm of each molecule was drawn and fit with a single-site specific binding model to get the apparent disassociation constant (K_d) and maximum adsorption (B_{max}) (that of **OGP-Cat** as in Figure 2B and others in Figure S2) from the adsorbed area mass at the respective concentrations. The results are summarized in Table

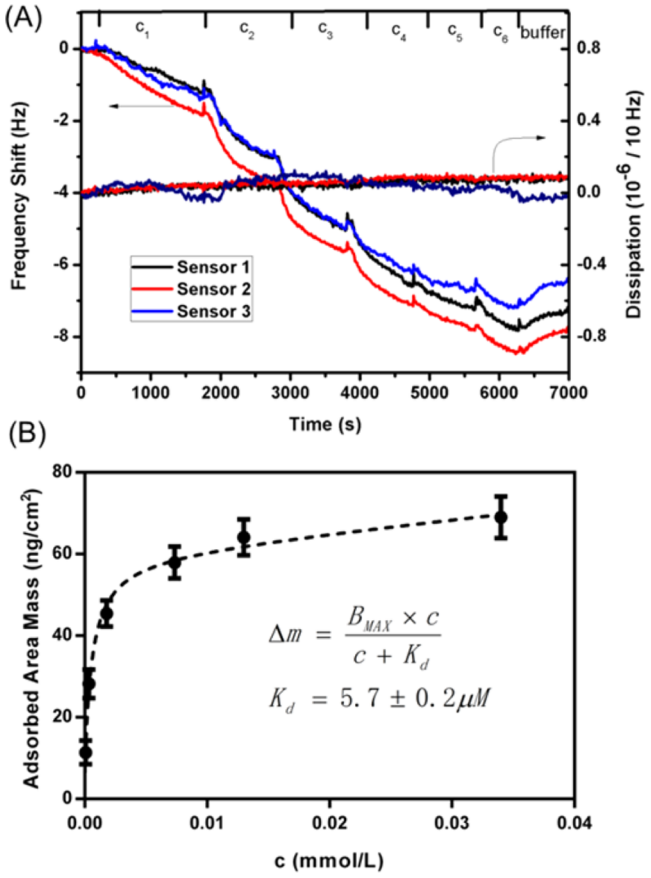

Figure 2. Adsorption of **OGP-Cat** onto TiO_2 surface and its adsorption isotherm. (A) The adsorption of **OGP-Cat** onto TiO_2 surface at different concentrations was measured by QCM-d, while the concentration was increased sequentially (c_1 = 0.068 μmol/L, c_2 = 0.34 μmol/L, c_3 = 1.8 μmol/L, c_4 = 7.3 μmol/L, c_5 = 13 μmol/L, and c_6 = 34 μmol/L). At last the adsorbed layer was washed with 25 mM HEPES buffer. The flow rate was 0.150 mL/min. Three independent measurements were shown. (B) The disassociation constant of **OGP-Cat** was 5.7 ± 0.2 μM by fitting the adsorption isotherm with single-site specific binding model, as representing with the dash line. The adsorbed area mass was calculated from Sauerbrey equation. Each dot with error bar was calculated on the basis of three independent measurements.

dx.doi.org/10.1021/ja508946h | J. Am. Chem. Soc. 2014, 136, 16357−16367

2. The K_d decreases as the valency changes from 1, to 2, and to 4. This clearly proved that multivalent binding ligands provide a stronger binding affinity. The enhancement parameters were calculated for the two series of molecules, with or without the PEG linkage. There is a 184-fold enhancement in binding affinity for **OGP-(Cat)$_4$** with the K_d of 31 ± 3 nM, when compared to **OGP-Cat**. Surprisingly, the PEG linkage also influences the binding affinity. When the valency equals 1 or 2, the molecules with PEG showed a 6-fold and 14-fold stronger binding compared with molecules without PEG. This is most likely because the PEG linkage serves as a spacer and weakens the effect of any intramolecular H-bond that may form between catechol groups and the OGP(10−14) peptide chain. From the quantification results of apparent K_d and B_{max}, for the tetravalent ligand, the binding is strong enough to saturate and sequester the whole molecule on TiO_2 surface at very low bioconjugate concentrations. A solution of **OGP-(Cat)$_4$** at 2.8 μM (100K_d) covers 99% of the binding sites on TiO_2 surfaces, at an OGP(10−14) concentration of 103 pmol/cm^2. The immobilization procedure simply involves immersing the TiO_2 surface in the solution for more than 2 h.

Table 2. Apparent Disassociation Constant (K_d), Maximum Adsorption (B_{max}), and Enhancement Parameter (β) of Catechol-Functionalized Dendrons to TiO_2 Surface

ligands to TiO_2	K_d (μM)[a]	B_{max} (ng/cm^2)[a]	β[b]
OGP-Cat	5.7 ± 0.2	54 ± 4	–
OGP-PEG-Cat	1.0 ± 0.1	59 ± 2	–
OGP-(Cat)$_2$	1.1 ± 0.3	55 ± 3	5
OGP-PEG-(Cat)$_2$	0.08 ± 0.01	73 ± 4	12
OGP-(Cat)$_4$	0.031 ± 0.003	160 ± 6	184
OGP-PEG-(Cat)$_4$	0.028 ± 0.008	196 ± 23	36

[a]Adsorption isotherm was fit with single-site specific binding model, $\Delta m = ((B_{max} \times C)/(K_d + C))$ where Δm is the amount of adsorbed analyte, c is the concentration of the analyte solution, B_{max} is the maximum adsorption, and K_d is the apparent dissociation constant. [b]Enhancement parameter is defined as the ratio of association constant of multivalent ligand to that of monovalent ligand, $\beta = (K_{a,multi}/K_{a,mono})$, and it was calculated on the basis of two sets of molecules with or without PEG linkage.

Binding Ability of OGP-(Cat)$_4$ to Versatile Surfaces. The adsorption of tetravalent binding ligand **OGP-(Cat)$_4$** to a wide range of materials was tested to identify the common features of materials that catechol-bearing ligands strongly bind to. As shown in Figure 3, **OGP-(Cat)$_4$** showed the strongest binding to CeO_2, TiO_2 and ZrO_2, strong binding to iron oxide (Fe_3O_4 and Fe_2O_3), some adsorption to gold, and weak adsorption to SiO_2. This is because the coordination bond between catechol and metals with empty *d*-orbitals or *f*-orbitals provides a stronger interaction than Hydrogen bonding. Limited adsorption of **OGP-(Cat)$_4$** with materials of compounds from main group elements, including SiO_2, Al_2O_3 and hydroxyapatite (HA), was confirmed even when applying a solution at 10-times higher concentration (Figure S3). Stronger adsorption was observed for transition metal and transition metal oxide, which was attributed to coordination bonding. Despite the strong binding with TiO_2, **OGP-(Cat)$_4$** showed similar strong binding affinity and persistence under buffer washing to other biomaterial-related surfaces, including zirconia, ZrO_2, a widely used material in prosthetic devices, cerium oxide, CeO_2, and iron oxide, Fe_3O_4. Therefore, we envision **OGP-(Cat)$_4$** as highly useful for the functionalization of transition metal oxides.

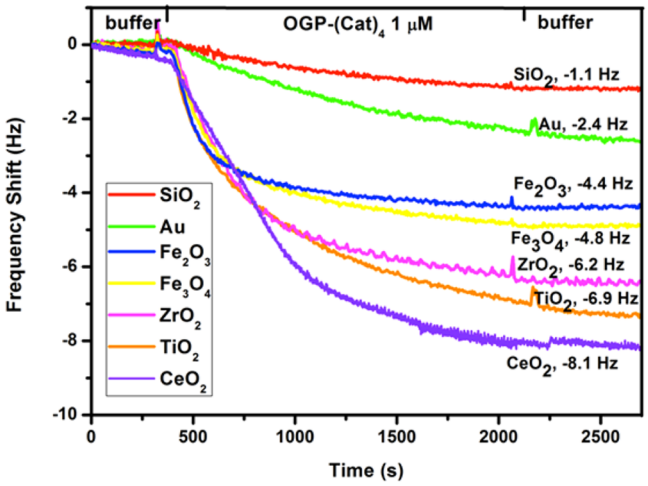

Figure 3. Tetravalent binding ligand **OGP-(Cat)$_4$** (c = 1 μM) shows strong binding affinities to versatile metal and metal oxide surfaces due to coordination bond, including Fe_2O_3, Fe_3O_4, ZrO_2, TiO_2 and CeO_2 surfaces as measured by QCM-d.

OGP-(Cat)$_n$ on TiO_2 Surface. To directly prove the existence of **OGP-(Cat)$_n$** on TiO_2 surface, XPS and fluorescein labeling experiments were carried out. The TiO_2 layer was prepared by RF sputter coating on glass slides or silica wafers. The thickness of TiO_2 layer was measured to be around 36 nm with O/Ti ratio equaling to 2.0 (Figure S4 and Figure S5). The surfaces roughness of deposited TiO_2 was measured by atomic force microscopy (AFM) with an RMS roughness around 1 nm (Figure S6).

Immobilization of peptides onto TiO_2 surfaces was completed by immersing the TiO_2 substrates into the corresponding modular peptide solution and incubating overnight at ambient temperature. The successful immobilization of **OGP-Cat** and **OGP-(Cat)$_4$** onto TiO_2-coated substrates were confirmed by XPS. Nitrogen is the element contained only in the modular peptides while not in bare TiO_2, as shown in the XPS survey scan of bare TiO_2 and **OGP-(Cat)$_4$** in Figure 4A. Thus, N 1s signal at 400.3 eV corresponding to the amide in peptides can be used to prove the immobilization of **OGP-(Cat)$_4$** onto TiO_2 surfaces (Figure 4A). The adsorbed **OGP-(Cat)$_4$** layer was readily removed with Ar^+ plasma treatment for 1 min, indicating that the N 1s indeed came from the very top adsorbed peptides layer (Figure 4B). It is noted that the N 1s peaks in Figure 4B are normalized to the highest intensity (O 1s) for comparison of the signal-to-noise ratio.

To quantify the increase in nitrogen due to adsorption of **OGP-Cat** and **OGP-(Cat)$_4$**, the nitrogen content (N 1s) was normalized with Ti content (Ti 2p), and compared with TiO_2 substrate after incubation in HEPES buffer overnight (TiO_2 as control), as shown in Table 3. The N/Ti ratio increased from 0.03 (TiO_2 control) to around 0.4 (**OGP-Cat**: 0 h incubation in buffer, **OGP-(Cat)$_4$**: 0 day incubation). The presence of modular peptide **OGP-(Cat)$_4$** was further proven by the significant change of C 1s and O 1s signatures in high resolution XPS spectra before and after the immobilization. In Figure 4C and 4D, the C 1s signals were fit with Gaussian model into three components based on their respective binding energy, including carbon of C−C bond (C1, 284.8 eV), of C−O bond (C2, 286.1 eV), and of amide bond (C3, 287.8 eV).

dx.doi.org/10.1021/ja508946h | J. Am. Chem. Soc. 2014, 136, 16357−16367

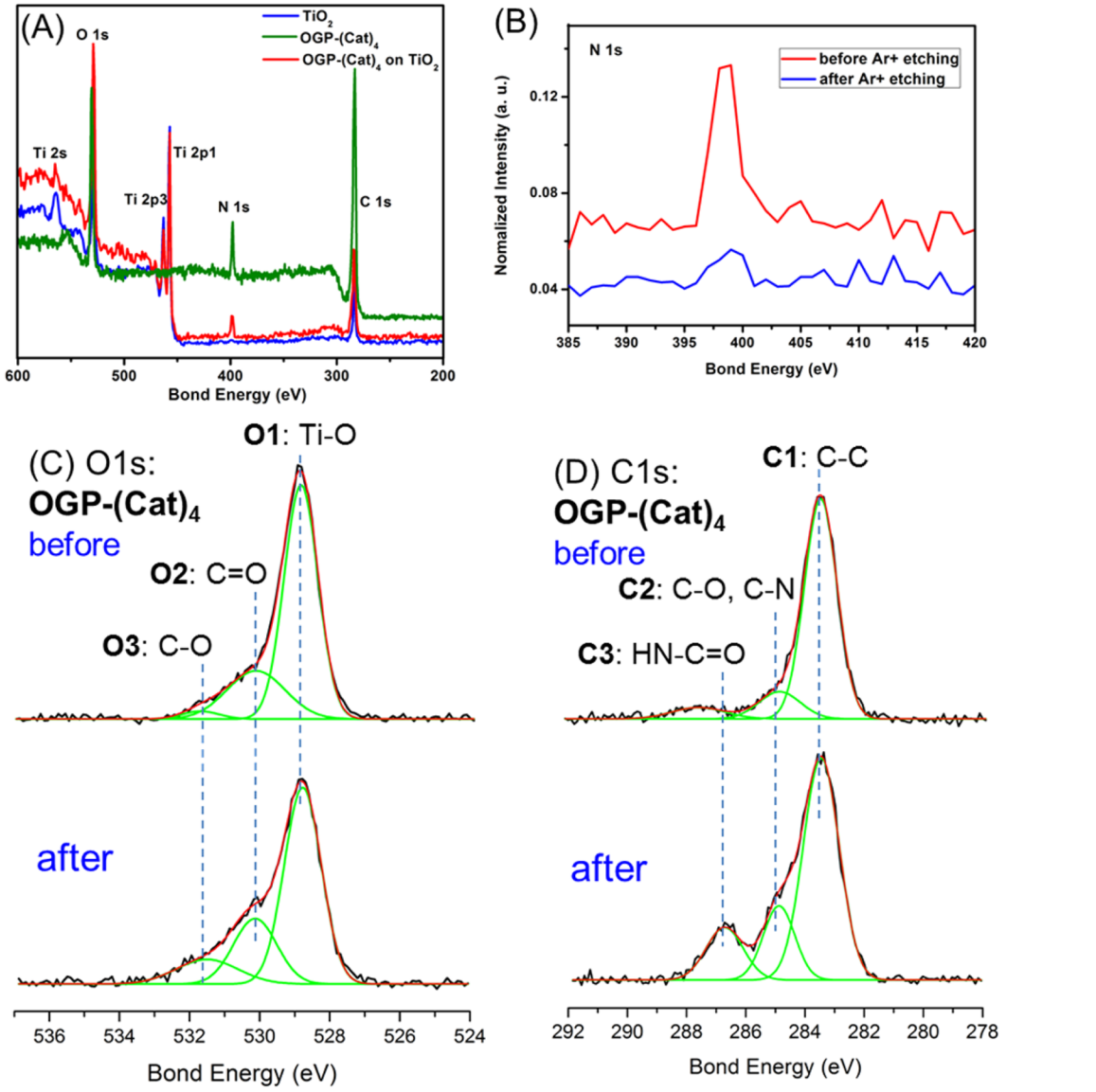

Surface	C2/C1	C3/C1	O2/O1	O3/O1	C3/N
bare TiO2	0.16	0.08	0.35	0.04	∞
OGP-(Cat)$_4$ on TiO$_2$	0.24	0.29	0.39	0.21	0.93

Figure 4. XPS characterization confirmed the successful immobilization of **OGP-(Cat)$_4$** on TiO_2 surface. (A) Survey scan of bare TiO_2 surface, **OGP-(Cat)$_4$**, and **OGP-(Cat)$_4$** immobilized TiO_2. The N 1s signal comes from amide bonds in peptides. (B) 1 min of Ar^+ plasma treatment to the **OGP-(Cat)$_4$** immobilized TiO_2 surface removed the adsorbed **OGP-(Cat)$_4$** layer. The N 1s peaks are normalized to the highest intensity (O 1s) for comparison of the signal-to-noise ratio. The signal changes in high resolution XPS spectra of O 1s (C) and C 1s (D) demonstrates the successful immobilization of **OGP-(Cat)$_4$** on TiO_2 substrates. The multiple peaks were fitted with a Gaussian model. The atomic ratios of C2/C1, C3/C1, O2/O1, O3/O1 and C3/N of respective surfaces were calculated on the basis of the integrated area of each peak.

Table 3. Immobilization of OGP-Cat and OGP-(Cat)$_4$ and Their Retention on TiO_2 Substrates[a,b,c]

surface	TiO_2		OGP-Cat on TiO_2			OGP-(Cat)$_4$ on TiO_2			
buffer incubation time	0 h (bare)	12 h (control)	0 h	12 h	36 h	0 day	3 day	7 day	14 day
N/Ti	0	0.03	0.41	0.34	0.21	0.43	0.44	0.45	0.24

[a]Atomic Ratios of N/Ti for the TiO_2 surface, the surfaces after **OGP-Cat** and **OGP-(Cat)$_4$** immobilization, and the **OGP-Cat** and **OGP-(Cat)$_4$** bearing surfaces after incubation in HEPES buffer. [b]Standard deviations are typically below 10% relative. [c]0 h incubation in 25 mM HEPES buffer (pH = 7.41 at 25 °C) means surfaces just after TiO_2 coating or **OGP-(Cat)$_n$** (n = 1,4) immobilization without incubation in buffer.

dx.doi.org/10.1021/ja508946h | J. Am. Chem. Soc. 2014, 136, 16357−16367

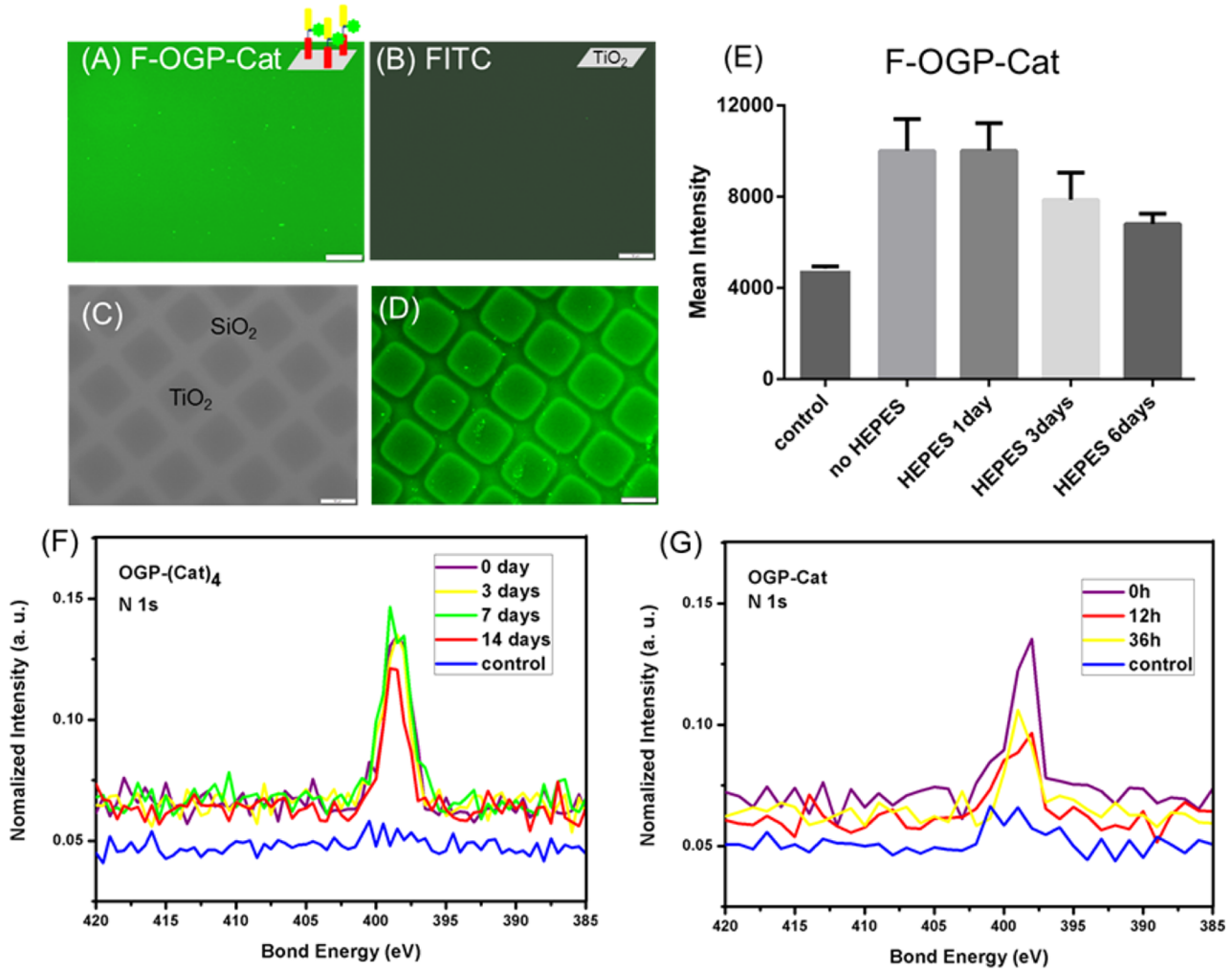

Figure 5. Immobilization of modular peptides was viewed by labeling the peptide with fluorescein, and due to multivalent binding effect, the retention time of **OGP-(Cat)$_4$** on titanium oxide surface in buffer at physiological pH was longer than 2 weeks, which is long enough to trigger the cell responses. (A–E) The immobilized **FITC-labeled OGP-Cat** on TiO_2 surface was observed under fluorescence microscope, and the mean intensity of fluorescence decreased after incubating the substrates in pH = 7.4 25 mM HEPES buffer due to the diffusion of **FITC-labeled OGP-Cat**. TiO_2 substrates were incubated in the solution of 0.5 mM (A) **FITC-labeled OGP-Cat** and (B) FITC overnight, then thoroughly washed with water and dried with N_2. **FITC-labeled OGP-Cat** immobilized TiO_2 pattern on glass slides observed under (C) bright field microscope and (D) fluorescence microscope. The scale bar is 50 μm. (E) Mean intensity of **FITC-labeled OGP-Cat** immobilized surface after incubation for different duration. The control sample is incubating TiO_2 substrates in the solution of FITC for overnight. The mean intensity was calculated on the basis of 10 randomly chosen sites observed under the same conditions. (F,G) The immobilized **OGP-(Cat)$_4$** preserved on the surface for more than 2 weeks in buffer at physiological pH, in comparison, the diffusion of monovalent ligand **OGP-Cat** was detected after 12 h. XPS spectra of N 1s signals taken after incubation of (F) **OGP-(Cat)$_4$** and (G) **OGP-Cat** immobilized TiO_2 substrates in HEPES buffer (pH = 7.4) for different duration, respectively. The control is taken after incubation of TiO_2 substrates in 25 mM HEPES buffer. To compare the signal-to-noise ratio, all spectra were normalized to the peak of highest intensity (O 1s).

Similarly, the O 1s signals were deconvoluted into three peaks: oxygen of Ti–O bond (O1, 530.2 eV), of C═O bond (O2, 531.5 eV), and of C–O bond (O3, 533.0 eV). The significant increase in the atomic ratios of C2/C1, C3/C1, O2/O1, and O3/O1 (table inserted in Figure 4) indicates the amide bonds and phenol rings contained in the **OGP-(Cat)$_4$**. The C3/N ratio, from amide bond of **OGP-(Cat)$_4$**, is 0.93, which is closed to the theoretical value of 1.

Fluorescein-labeled modular peptide **FITC-labeled OGP-Cat** was also synthesized to visualize the presence of the immobilized peptides on TiO_2 surface using fluorescence microscopy. After immobilization of **FITC-labeled OGP-Cat** onto TiO_2 surfaces, the fluorescence intensity was much stronger compared to the control sample, which incubating TiO_2-coated substrates in a solution of FITC at identical concentration, as shown in Figure 5A and 5B. When a TiO_2 pattern was present on the glass slides, it was observed that the TiO_2 region showed a significantly stronger fluorescence signal due to the stronger binding affinity of **FITC-labeled OGP-Cat** to TiO_2 compared with SiO_2, Figure 5C and Figure 5D.

Retention of OGP-(Cat)$_n$ on TiO_2 Surface. To study the stability of sequestered modular peptides on targeting surfaces, the modular peptide immobilized TiO_2 substrates were immersed in 25 mM HEPES buffer (pH= 7.4 at 25 °C) and incubated for different duration, respectively. The mean intensity of **FITC-labeled OGP-Cat** immobilized TiO_2 substrates after incubation was quantified to detect the diffusion of **FITC-labeled OGP-Cat** into surrounding solution, Figure 5E. After 3 days incubation, the intensity deceased by about a half of the original intensity coming from **FITC-labeled OGP-**

dx.doi.org/10.1021/ja508946h | J. Am. Chem. Soc. 2014, 136, 16357–16367

Cat on surfaces, indicating the dissociation of monovalent ligand. Because the N 1s signals were assigned to the modular peptides, the decrease of N 1s corresponds to the dissociation of adsorbed peptides from TiO_2 surface. In Figure 5F, tetravalent ligand **OGP-(Cat)$_4$** showed a longer retention time on the targeted surface, the decrease of N 1s signal was not detected until after 14 days, while that of monovalent ligand **OGP-Cat** showed a reducing in N 1s signal after 12 h (Figure 5G). The atomic ratio of N/Ti were calculated, as shown in Table 3, the half-life time of immobilized **OGP-Cat** and **OGP-(Cat)$_4$** presenting on TiO_2 surface is around 36 h and 14 days, respectively. The mismatch of retention time of monovalent ligands was attributed to the sensitivity difference of XPS and fluorescence microscopy. The tetravalent ligands **OGP-(Cat)$_4$** are clearly present on the TiO_2 surface beyond 2 weeks, which is enough to trigger the cascade signaling reactions in adjacent cells.

Preferential Immobilization of OGP-(Cat)$_n$. We have shown that the catechol-bearing dendrons have strong binding to transition metal compounds due to coordination bond, while weak binding to materials when only H-bond or other weak noncovalent interactions exist. Thus, immersing materials with both SiO_2 and TiO_2 present on the surface into the solution of **OGP-(Cat)$_4$**, the **OGP-(Cat)$_4$** will preferentially adsorb onto TiO_2 region. This provides a method to preferentially functionalize selected regions on the surface, which is useful in the fabrication of surfaces with locally restricted functionality of peptides. It was demonstrated with a partially coated glass slides containing SiO_2 region in the middle and TiO_2 in the surrounding region. After incubating the slides in the solution of **OGP-(Cat)$_4$** (c = 1 μM) overnight, the elements present on the surface in the respective regions were detected by XPS. As shown in Figure 6, the green spots are positions where X-ray was directed on the surface. The signals from SiO_2 and TiO_2 regions are quite different. The local existence of Si and Ti was confirmed in XPS. And notably, the TiO_2 region showed a much stronger signal in N 1s, which corresponds to the adsorbed **OGP-(Cat)$_4$**. The atomic percentage of nitrogen from N 1s in TiO_2 and SiO_2 region were 8 ± 1% and 1.7 ± 0.8%, respectively.

Cytotoxicity. MC3T3-E1 cells were seeded on the TiO_2 substrates with immobilized **FITC-labeled OGP-Cat** and cultured for 24 h. Cell viability was studied (Figure S7). The dominant green fluorescence (viability >98%) from live cells in the live/dead cell staining demonstrates the modular peptide bioconjugates are not toxic when tethered to the surface. The cells were well spread on the peptide-bearing surfaces, which is a consistent with an adherent proliferating cell population.

XPS of OGP(10−14) Immobilized TiO_2-Coated Substrates. The loading amount was calculated on the basis of the adsorption isotherm fitted with signal site specific model as shown in Table 2. The XPS characterization was applied to detect the immobilized peptides from the N 1s signal, which is the element only contained in the amide bond in **OGP-PEG-(Cat)$_4$**. The nitrogen content normalized with total amount of elements on surface is 5.8 ± 0.3 for OGP-99% substrates, while that of OGP-50% is not distinguished from noise due to low content (Figure S8).

Effects of Immobilized OGP(10−14) on Cell Adhesion and Morphology. Because the capacity for cells to interact with growth factors is an important cell behavior,[71] the MC3T3-E1 cells were fluorescently stained to visualize actin and vinculin proteins, to assess the organization of cytoskeleton and the spatial distribution of focal adhesion contacts, respectively. After 24 h, the MC3T3-E1 cells were attached on both OGP-99% and bare TiO_2 substrates and the focal adhesion contacts between cells and substrates formed, as shown in Figure 7A and 7B. There is no statistic difference in cell area and aspect ratio for the cell adhesion to OGP-99% and bare TiO_2 substrates, because OGP peptides, immobilized or dissolved, show no effects in the adhesion of MC3T3-E1 cells as described in our previous work.[2]

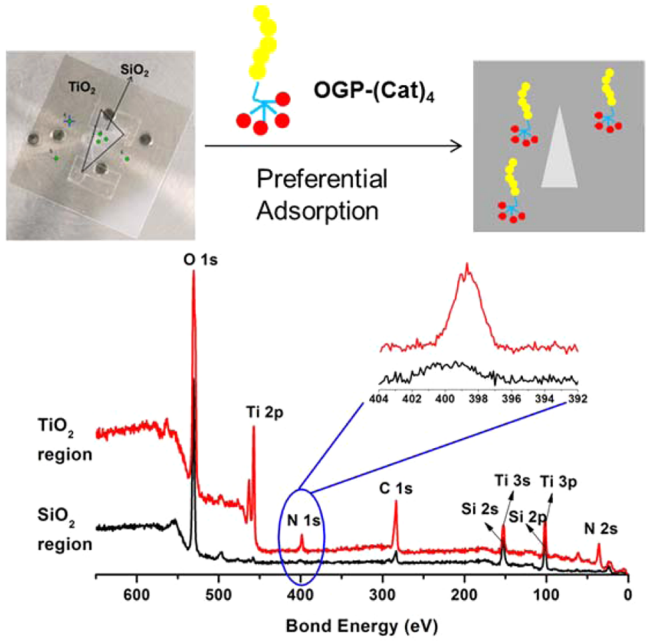

Figure 6. Preferential adsorption of **OGP-(Cat)$_4$** to the TiO_2 region of a partially TiO_2-coated glass slide observed with XPS. The green spots on the substrates are positions where XPS spectra were taken (three in SiO_2 region and three in TiO_2 region). The stronger signal of N 1s in the TiO_2 region compared with that of the SiO_2 region indicates peptides preferentially adsorbed to the TiO_2 surface. The XPS signals were normalized with the strongest peak intensity (O 1s). The atomic percentage of nitrogen in TiO_2 and SiO_2 region were 8 ± 1% and 1.7 ± 0.8%, respectively.

Effects of Immobilized OGP(10−14) on Cell Proliferation. The OGP-99%, OGP-50% and TiO_2 substrates were seeded with preosteoblast MC3T3-E1 cells with cell density of 18 cell/mm^2. In the first 24 h, the cells were mostly attaching to the surface and adjusting to the new environment; therefore, the cell number after 1 day for all three substrates was comparable. After 3 days, the MC3T3-E1 cells on OGP-99% substrates showed the highest cell number compared with the others, indicating that the OGP(10−14) peptide promoted a faster cell proliferation rate in a concentration dependent manner, as shown in Figure 7.

Effects of Immobilized OGP(10−14) on Osteogenic Differentiation. Bone sialoprotein (BSP) constitutes approximately 8% of all noncollagenous proteins found in bone, and is important in the nucleation process of hydroxyapatite formation.[72] Osteocalcin (OCN) is expressed solely by the osteoblast; thus, it is the most specific protein for osteoblast differentiation and mineralization.[73] The fluorescent staining of BSP and OCN, the maker proteins of osteogenic differentiation, reveals that the MC3T3-E1 cells on the OGP-99%, OGP-50% and TiO_2 substrates secreted abundant amounts of BSP and OCN after 2 weeks, as indicated by the strong

dx.doi.org/10.1021/ja508946h | J. Am. Chem. Soc. 2014, 136, 16357−16367

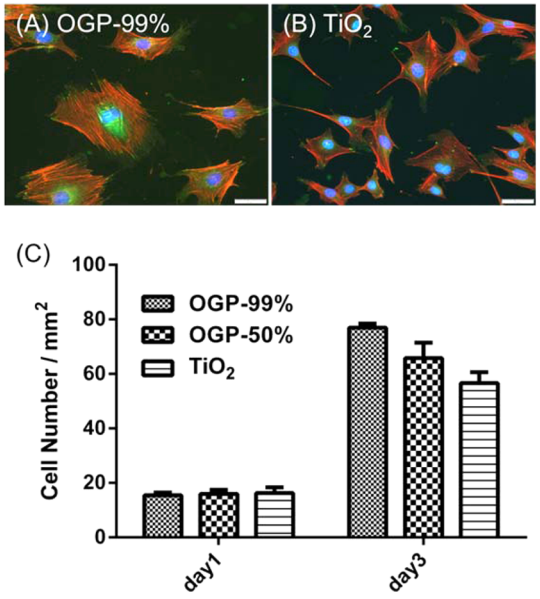

Figure 7. Adhesion of MC3T3-E1 cells were not significantly influenced by the immobilized OGP(10−14) peptides, while they proliferated faster on OGP-bearing surface with dose-dependency. After 24 h, MC3T3-E1 cells were well spread on substrates with or without immobilized OGP(10−14) and formed focal adhesion contacts with the substrates, as indicating by the immunohistochemical staining of adherent cells on (A) OGP-99% and (B) bare TiO_2 substrates. Red corresponds to F-actin in cytoskeleton; green corresponds to vinculin in focal adhesion complex; and blue corresponds to the nuclei (scale bar is 50 μm). (C) The immobilized **OGP-PEG-(Cat)$_4$** promoted the cell proliferation, and this effect was dose-dependent. Cell number on substrates after day 1 and day 3 were evaluated by PrestoBlue Assay. The error bar was calculated from three replicates.

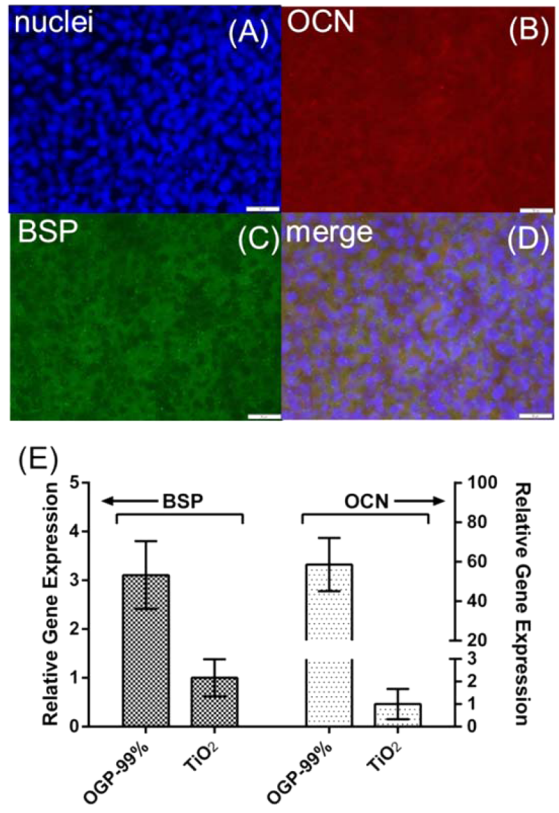

Figure 8. Bone sialoprotein (BSP) and osteocalcin (OCN), late markers of differentiation to osteoblast, were secreted by MC3T3-E1 cells on OGP-99% substrate, as demonstrated by the immunohistochemical staining after 2 weeks. (A) blue corresponds to the nuclei; (B) red corresponds to osteocalcin (OCN); (C) green corresponds to bone sialoprotein (BSP); and (D) is the merged image of the three channels (scale bar = 50 μm). Similar results were observed on OGP-50% and TiO_2 substrates. However, the cells on OGP-99% substrate expressed a much higher gene level of BSP and OCN, compare to cells on bare TiO_2, as shown in the (E) mRNA levels of transcription factor genes of BSP and OCN, in MC3T3-E1 cells measured by real-time PCR after cell culture for 18 days. Data represent relative expression to the level of the control (cells on TiO_2), set at 1, and mean value and standard deviation calculated from triplicates.

fluorescence of red (OCN) and green (BSP) on the substrates. In Figure 8, the immunohistochemical staining of cells on OGP-99% substrates is shown. Similar results were observed for OGP-50% and TiO_2 substrates. From the enlarged images, a difference in the distribution of OCN and BSP was observed. The amount of BSP in the cytoplasm and extracellular matrix (ECM) is similar (Figure S9A), while the OCN showed a higher concentration in the cytoplasm (Figure S9B). This is consistent with the fact that BSP is a component in bone matrix, while OCN is secreted by osteoblasts to regulate the metabolic activities and bone-building process.[73] Using RT-PCR, a quantitative comparison of the expressed mRNA level of BSP and OCN demonstrated a significant increase in expression of these osteogenic genes in cells on OGP-99% substrates. With enough OGP(10−14) present on the surface, the osteogenic differentiation of MC3T3-E1 cells was enhanced.

Effects of Immobilized OGP(10−14) on ALP Activity. Alkaline phosphatase (ALP) plays a critical role in the process of mineral formation in tissues such as bone, cartilage, and dentin.[74] ALP activity is the most widely recognized biochemical marker for bone forming ability. A standard colorimetric assay was performed to quantify the ALP activity after culture for 18 days, and the values were normalized with total amount of protein to account for the difference of cell number in samples. The immobilized OGP(10−14) at high concentrations exhibited an enhancement effect on the ALP activity (Figure 9A). MC3T3-E1 cells on OGP-99% showed a 3-fold higher ALP level compared with those on OGP-50% and TiO_2. This up-regulation of ALP activity indicates the immobilized OGP(10−14) preserves its ability to stimulate the dephosphorylation, which is an essential activity involved in the mineralization process. The mRNA expression level of ALP in cells on OGP-99% is also higher in comparison with those on OGP-50% and TiO_2 as indicated in RT-PCR (Figure 9B).

Effects of Immobilized OGP(10−14) on Mineralization. The appearance of calcium deposition is the phenotypic marker for the last stage of mature osteoblast. The extent of mineralized extracellular matrix (ECM) formed on OGP-99%, OGP-50% and TiO_2 substrates after 2 weeks was examined by staining with Alizarin Red S., a red dye that forms a complex with calcium depositions in ECM.[75] The cell films on all three substrates were positively stained red, indicating the MC3T3-E1 cells differentiated to osteoblast and secreted mineralized ECM. Under the microscope, the mineralized osteoids, spherulites with dark red color, ranging from 0.5 to 2 μm, were observed on all three substrates (Figure 9D, 9E and 9F). But only cell films on OGP-99% substrates showed the dark mineralized chunks, ranging from 2 to 10 μm, which is

dx.doi.org/10.1021/ja508946h | J. Am. Chem. Soc. 2014, 136, 16357−16367

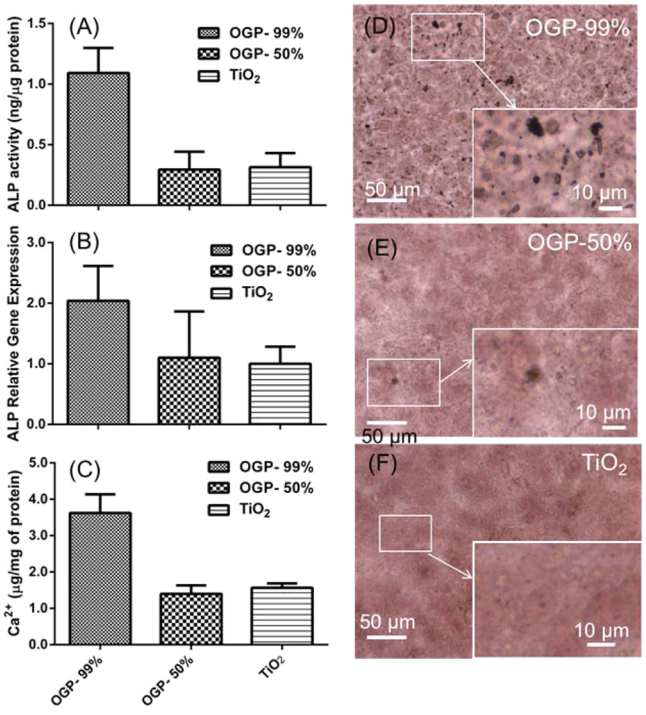

Figure 9. Immobilized OGP(10−14) peptide on OGP-99% substrates up-regulated the alkaline phosphatase (ALP) activity and mineralization of MC3T3 cells. (A,B) The ALP activity and its mRNA level of MC3T3 cells on OGP-99% substrate was significantly higher compared to substrates with lower concentration or none. (A) ALP activity of MC3T3 cells cultured on OGP-99%, OGP-50%, and TiO_2 substrates, respectively, on day 18. (B) mRNA levels of transcription factor gene of ALP, in MC3T3-E1 cells measured by real-time PCR after cell culture for 18 days. (C) Ca^{2+} accumulation in the cell films quantified with ICP-OES and normalized with total amount of protein. The cell films on OGP-99% exhibited 2-fold higher content of Ca^{2+} compared with those on other substrates. The error bar was calculated from three replicates. (D−F) Mineralization of MC3T3-E1 cells on substrates studied by Alizarin Red S. staining on day 14 and Ca^{2+} quantification by ICP-AES on day 18. Larger sized calcified nodules were observed on OGP-99%, indicating promoted mineralization results from the higher concentration of OGP(10−14). Images of cell films on (D) OGP-99%, (E) OGP-50%, and (F) TiO_2 substrates after Alizarin Red S. observed under bight field microscope. The mineralized osteoids, the spherulites with dark red color, ranging from 0.5 to 2 μm, were observed on all the three kinds of substrates. And only cell films on OGP-99% showed the dark mineralized chunks, ranging from 2 to 10 μm.

attributed to the higher content of calcium in the cell films on OGP-99% substrates. The calcium content was quantified with ICP-OES after 18 days culture in nonosteogenic medium. The result is consistent with that of Alizarin Red S. staining, as show in Figure 9C. The cell films on OGP-99% substrates exhibited more than two times higher concentration of Ca^{2+} normalized by total amount of protein to account for the difference in cell numbers. Therefore, the immobilized OGP(10−14) on surfaces promotes the mineralization of osteoblasts.

CONCLUSION

Using straightforward synthesis, a series of multivalent catechol-bearing modular peptides were generated with the aim of providing a simple and efficient method to functionalize metal-oxide based orthopaedic implants with bioactive peptides. With a multivalent binding strategy, tetravalent ligands were shown to persist on the metal oxide surfaces in vitro beyond 2 weeks under near physiological conditions. The bioactivity of immobilized peptides was demonstrated in an in vitro cell culture study. The tethered OGP(10−14) promoted the proliferation, osteogenic differentiation and mineralization of MC3T3-E1 cells. Considering their strong adhesion to versatile metal oxide surfaces, this modular peptide strategy is promising for the development of translational implants with improved bioactivity.

ASSOCIATED CONTENT

Supporting Information

Experimental details for catechol-functionalized peptides synthesis, surface adsorption measurement, adsorption isotherm analysis, surface modification and characterization, and cell culture study; MS data of target molecules; adsorption isotherm of ligands binding to TiO_2; weak adsorption of **OGP-(Cat)$_4$** to other surfaces; characterization of TiO_2 deposition obtained by RF sputtering coating; Live/dead assay; XPS data of substrates in cell culture study; and immunochemical staining of BSP and OCN in high magnification. This material is available free of charge via the Internet at http://pubs.acs.org.

AUTHOR INFORMATION

Corresponding Author

becker@uakron.edu

Notes

The authors declare no competing financial interest.

ACKNOWLEDGMENTS

The authors thank Richard Fowler and Harpal Singh for help with RF sputtering coating, Jukuan Zheng for precursor synthesis, Dr. Thomas Leeper for use of an HPLC purification system and Dr. Nikolov Zhorro for the help in XPS characterization. This work was supported by the National Science Foundation (DMR-1105329) and a seed grant from the Austen Bioinnovation Institute in Akron.

REFERENCES

(1) Hersel, U.; Dahmen, C.; Kessler, H. *Biomaterials* **2003**, *24*, 4385.
(2) Moore, N. M.; Lin, N. J.; Gallant, N. D.; Becker, M. L. *Biomaterials* **2010**, *31*, 1604.
(3) He, X.; Ma, J.; Jabbari, E. *Langmuir* **2008**, *24*, 12508.
(4) Moore, N. M.; Lin, N. J.; Gallant, N. D.; Becker, M. L. *Acta Biomater.* **2011**, *7*, 2091.
(5) Tsurkan, M. V.; Chwalek, K.; Prokoph, S.; Zieris, A.; Levental, K. R.; Freudenberg, U.; Werner, C. *Adv. Mater.* **2013**, *25*, 2606.
(6) Kim, J.; Kim, I. S.; Cho, T. H.; Lee, K. B.; Hwang, S. J.; Tae, G.; Noh, I.; Lee, S. H.; Park, Y.; Sun, K. *Biomaterials* **2007**, *28*, 1830.
(7) Shekaran, A.; Garcia, J. R.; Clark, A. Y.; Kavanaugh, T. E.; Lin, A. S.; Guldberg, R. E.; Garcia, A. J. *Biomaterials* **2014**, *35*, 5453.
(8) Garty, S.; Kimelman-Bleich, N.; Hayouka, Z.; Cohn, D.; Friedler, A.; Pelled, G.; Gazit, D. *Biomacromolecules* **2010**, *11*, 1516.
(9) Lin, F.; Zheng, J.; Yu, J.; Zhou, J.; Becker, M. L. *Biomacromolecules* **2013**, *14*, 2857.
(10) Sargeant, T. D.; Rao, M. S.; Koh, C. Y.; Stupp, S. I. *Biomaterials* **2008**, *29*, 1085.
(11) Khoo, X.; Hamilton, P.; O'Toole, G. A.; Snyder, B. D.; Kenan, D. J.; Grinstaff, M. W. *J. Am. Chem. Soc.* **2009**, *131*, 10992.
(12) Micksch, T.; Liebelt, N.; Scharnweber, D.; Schwenzer, B. *ACS Appl. Mater. Interfaces* **2014**, *6*, 7408.
(13) Amin Yavari, S.; van der Stok, J.; Chai, Y. C.; Wauthle, R.; Tahmasebi Birgani, Z.; Habibovic, P.; Mulier, M.; Schrooten, J.; Weinans, H.; Zadpoor, A. A. *Biomaterials* **2014**, *35*, 6172.

(14) Hisbergues, M.; Vendeville, S.; Vendeville, P. *J. Biomed. Mater. Res., Part B* **2009**, *88B*, 519.
(15) Patil, S.; Sandberg, A.; Heckert, E.; Self, W.; Seal, S. *Biomaterials* **2007**, *28*, 4600.
(16) Das, M.; Patil, S.; Bhargava, N.; Kang, J. F.; Riedel, L. M.; Seal, S.; Hickman, J. J. *Biomaterials* **2007**, *28*, 1918.
(17) Pankhurst, Q. A.; Connolly, J.; Jones, S. K.; Dobson, J. *J. Phys. D: Appl. Phys.* **2003**, *36*, R167.
(18) Meyers, S. R.; Grinstaff, M. W. *Chem. Rev.* **2011**, *112*, 1615.
(19) Pan, J.; Liao, H.; Leygraf, C.; Thierry, D.; Li, J. *J. Biomed. Mater. Res.* **1998**, *40*, 244.
(20) Jung, H.-D.; Yook, S.-W.; Han, C.-M.; Jang, T.-S.; Kim, H.-E.; Koh, Y.-H.; Estrin, Y. *J. Biomed. Mater. Res., Part B* **2014**, *102*, 913.
(21) Bronk, J. K.; Russell, B. H.; Rivera, J. J.; Pasqualini, R.; Arap, W.; Hook, M.; Barbu, E. M. *Acta Biomater.* **2014**, *10*, 3354.
(22) VandeVondele, S.; Voros, J.; Hubbell, J. A. *Biotechnol. Bioeng.* **2003**, *82*, 784.
(23) Christensen, T. J.; Annis, P.; Hohl, J. B.; Patel, A. A. *Spine J.* **2014**, *14*, E23.
(24) Carragee, E. J.; Hurwitz, E. L.; Weiner, B. K. *Spine J.* **2011**, *11*, 471.
(25) Cahill, K. S.; Chi, J. H.; Day, A.; Claus, E. B. *JAMA, J. Am. Med. Assoc.* **2009**, *302*, 58.
(26) Chen, N. F.; Smith, Z. A.; Stiner, E.; Armin, S.; Sheikh, H.; Khoo, L. T. *J. Neurosurg.: Spine* **2010**, *12*, 40.
(27) Balasundaram, G.; Yao, C.; Webster, T. J. *J. Biomed. Mater. Res., Part A* **2008**, *84A*, 447.
(28) Wall, I.; Donos, N.; Carlqvist, K.; Jones, F.; Brett, P. *Bone* **2009**, *45*, 17.
(29) Bagno, A.; Piovan, A.; Dettin, M.; Chiarion, A.; Brun, P.; Gambaretto, R.; Fontana, G.; Di Bello, C.; Palu, G.; Castagliuolo, I. *Bone* **2007**, *40*, 693.
(30) Seol, Y. J.; Park, Y. J.; Lee, S. C.; Kim, K. H.; Lee, J. Y.; Kim, T. I.; Lee, Y. M.; Ku, Y.; Rhyu, I. C.; Han, S. B.; Chung, C. P. *J. Biomed. Mater. Res., Part A* **2006**, *77A*, 599.
(31) Lee, H.; Dellatore, S. M.; Miller, W. M.; Messersmith, P. B. *Science* **2007**, *318*, 426.
(32) Liu, L.-M.; Li, S.-C.; Cheng, H.; Diebold, U.; Selloni, A. *J. Am. Chem. Soc.* **2011**, *133*, 7816.
(33) Ye, Q.; Zhou, F.; Liu, W. *Chem. Soc. Rev.* **2011**, *40*, 4244.
(34) Yu, J.; Wei, W.; Menyo, M. S.; Masic, A.; Waite, J. H.; Israelachvili, J. N. *Biomacromolecules* **2013**, *14*, 1072.
(35) Wei, Q.; Becherer, T.; Noeske, P.-L. M.; Grunwald, I.; Haag, R. *Adv. Mater.* **2014**, *26*, 2688.
(36) Matos-Pérez, C. R.; White, J. D.; Wilker, J. J. *J. Am. Chem. Soc.* **2012**, *134*, 9498.
(37) Sedó, J.; Saiz-Poseu, J.; Busqué, F.; Ruiz-Molina, D. *Adv. Mater.* **2013**, *25*, 653.
(38) Lee, H.; Lee, K. D.; Pyo, K. B.; Park, S. Y.; Lee, H. *Langmuir* **2010**, *26*, 3790.
(39) Na, H. B.; Palui, G.; Rosenberg, J. T.; Ji, X.; Grant, S. C.; Mattoussi, H. *ACS Nano* **2011**, *6*, 389.
(40) Gulley-Stahl, H.; Hogan, P. A.; Schmidt, W. L.; Wall, S. J.; Buhrlage, A.; Bullen, H. A. *Environ. Sci. Technol.* **2010**, *44*, 4116.
(41) Connor, P. A.; Dobson, K. D.; McQuillan, A. J. *Langmuir* **1995**, *11*, 4193.
(42) Gillich, T.; Benetti, E. M.; Rakhmatullina, E.; Konradi, R.; Li, W.; Zhang, A.; Schlüter, A. D.; Textor, M. *J. Am. Chem. Soc.* **2011**, *133*, 10940.
(43) Ham, H. O.; Park, S. H.; Kurutz, J. W.; Szleifer, I. G.; Messersmith, P. B. *J. Am. Chem. Soc.* **2013**, *135*, 13015.
(44) Lee, J. S.; Lee, J. S.; Wagoner-Johnson, A.; Murphy, W. L. *Angew. Chem., Int. Ed.* **2009**, *48*, 6266.
(45) Lee, J. S.; Wagoner Johnson, A. J.; Murphy, W. L. *Adv. Mater.* **2010**, *22*, 5494.
(46) Lu, Y.; Lee, J. S.; Nemke, B.; Graf, B. K.; Royalty, K.; Illgen, R., III; Vanderby, R., Jr.; Markel, M. D.; Murphy, W. L. *PLoS One* **2012**, *7*, e50378.
(47) Zhu, H. B.; Guo, D. Z.; Yang, S. J.; Zhang, Y. H.; Wang, H.; Guo, H. T.; Zhang, Y.; Cheng, D. C. *Vet. Med. (Prague, Czech Repub.)* **2008**, *53*, 501.
(48) Badjic, J. D.; Nelson, A.; Cantrill, S. J.; Turnbull, W. B.; Stoddart, J. F. *Acc. Chem. Res.* **2005**, *38*, 723.
(49) Fasting, C.; Schalley, C. A.; Weber, M.; Seitz, O.; Hecht, S.; Koksch, B.; Dernedde, J.; Graf, C.; Knapp, E.-W.; Haag, R. *Angew. Chem., Int. Ed.* **2012**, *51*, 10472.
(50) Baldini, L.; Casnati, A.; Sansone, F.; Ungaro, R. *Chem. Soc. Rev.* **2007**, *36*, 254.
(51) Helms, B. A.; Reulen, S. W. A.; Nijhuis, S.; de Graaf-Heuvelmans, P.; Merkx, M.; Meijer, E. W. *J. Am. Chem. Soc.* **2009**, *131*, 11683.
(52) Mammen, M.; Choi, S. K.; Whitesides, G. M. *Angew. Chem., Int. Ed.* **1998**, *37*, 2755.
(53) Marradi, M.; Chiodo, F.; Garcia, I.; Penades, S. *Chem. Soc. Rev.* **2013**, *42*, 4728.
(54) Griffin, J. H.; Linsell, M. S.; Nodwell, M. B.; Chen, Q. Q.; Pace, J. L.; Quast, K. L.; Krause, K. M.; Farrington, L.; Wu, T. X.; Higgins, D. L.; Jenkins, T. E.; Christensen, B. G.; Judice, J. K. *J. Am. Chem. Soc.* **2003**, *125*, 6517.
(55) Boas, U.; Heegaard, P. M. H. *Chem. Soc. Rev.* **2004**, *33*, 43.
(56) Helms, B. A.; Reulen, S. W. A.; Nijhuis, S.; Graaf-Heuvelmans, P. T. H. M. d.; Merkx, M.; Meijer, E. W. *J. Am. Chem. Soc.* **2009**, *131*, 11683.
(57) Hong, S.; Leroueil, P. R.; Majoros, I. J.; Orr, B. G.; Baker, J. R., Jr.; Holl, M. M. B. *Chem. Biol.* **2007**, *14*, 107.
(58) Tang, W.; Ma, Y. R.; Xie, S. B.; Guo, K.; Katzenmeyer, B.; Wesdemiotis, C.; Becker, M. L. *Biomacromolecules* **2013**, *14*, 3304.
(59) Kramer, R. H.; Karpen, J. W. *Nature* **1998**, *395*, 710.
(60) Zanini, D.; Roy, R. *J. Am. Chem. Soc.* **1997**, *119*, 2088.
(61) Gestwicki, J. E.; Cairo, C. W.; Strong, L. E.; Oetjen, K. A.; Kiessling, L. L. *J. Am. Chem. Soc.* **2002**, *124*, 14922.
(62) Bastings, M. M. C.; Helms, B. A.; van Baal, I.; Hackeng, T. M.; Merkx, M.; Meijer, E. W. *J. Am. Chem. Soc.* **2011**, *133*, 6636.
(63) Huskens, J.; Mulder, A.; Auletta, T.; Nijhuis, C. A.; Ludden, M. J. W.; Reinhoudt, D. N. *J. Am. Chem. Soc.* **2004**, *126*, 6784.
(64) Krishnamurthy, V. M.; Semetey, V.; Bracher, P. J.; Shen, N.; Whitesides, G. M. *J. Am. Chem. Soc.* **2007**, *129*, 1312.
(65) Greenberg, Z.; Chorev, M.; Muhlrad, A.; Shteyer, A.; Namdarattar, M.; Casap, N.; Tartakovsky, A.; Vidson, M.; Bab, I. *J. Clin. Endocrinol. Metab.* **1995**, *80*, 2330.
(66) Chen, Z. X.; Chang, M.; Peng, Y. L.; Zhao, L.; Zhan, Y. R.; Wang, L. J.; Wang, R. *Regul. Pept.* **2007**, *142*, 16.
(67) Saska, S.; Scarel-Caminaga, R. M.; Teixeira, L. N.; Franchi, L. P.; dos Santos, R. A.; Gaspar, A.; de Oliveira, P. T.; Rosa, A.; Takahashi, C.; Messaddeq, Y.; Ribeiro, S. J. L.; Marchetto, R. *J. Mater. Sci.: Mater. Med.* **2012**, *23*, 2253.
(68) Stakleff, K. S.; Lin, F.; Callahan, L. A. S.; Wade, M. B.; Esterle, A.; Miller, J.; Graham, M.; Becker, M. L. *Acta Biomater.* **2013**, *9*, 5132.
(69) Horii, A.; Wang, X. M.; Gelain, F.; Zhang, S. G. *PLoS One* **2007**, *2*, 9.
(70) Lu, T. L.; Chen, T.; Zhai, Y. K.; Ma, Y. F.; Xiao, Y. H. *Soft Mater.* **2014**, *12*, 79.
(71) Gumbiner, B. M. *Cell* **1996**, *84*, 345.
(72) Ganss, B.; Kim, R. H.; Sodek, J. *Crit. Rev. Oral Biol. Med.* **1999**, *10*, 79.
(73) Lee, N. K.; Sowa, H.; Hinoi, E.; Ferron, M.; Ahn, J. D.; Confavreux, C.; Dacquin, R.; Mee, P. J.; McKee, M. D.; Jung, D. Y.; Zhang, Z.; Kim, J. K.; Mauvais-Jarvis, F.; Ducy, P.; Karsenty, G. *Cell* **2007**, *130*, 456.
(74) Hessle, L.; Johnson, K. A.; Anderson, H. C.; Narisawa, S.; Sali, A.; Goding, J. W.; Terkeltaub, R.; Millan, J. L. *Proc. Natl. Acad. Sci. U. S. A.* **2002**, *99*, 9445.
(75) Puchtler, H.; Meloan, S. N.; Terry, M. S. *J. Histochem. Cytochem.* **1969**, *17*, 110.